optica

Q-plate enabled spectrally diverse orbital-angular-momentum conversion for stimulated emission depletion microscopy

L. Yan,[1] P. Gregg,[1] E. Karimi,[2] A. Rubano,[3] L. Marrucci,[3] R. Boyd,[2,4] and S. Ramachandran[1,*]

[1]Department of Electrical and Computer Engineering, Boston University, Boston, Massachusetts 02215, USA
[2]Department of Physics, University of Ottawa, 25 Templeton, Ottawa, Ontario K1N 6N5, Canada
[3]Dipartimento di Fisica, Università di Napoli Federico II and CNR-SPIN via Cintia, 80126 Napoli, Italy
[4]Institute of Optics, University of Rochester, Rochester, New York 14627, USA
*Corresponding author: sidr@bu.edu

Received 21 July 2015; revised 8 September 2015; accepted 10 September 2015 (Doc. ID 246297); published 12 October 2015

Spin to orbital angular momentum (OAM) conversion using a device known as a q-plate has gained recent attention as a convenient means of creating OAM beams. We show that the dispersive properties of a $q = 1/2$ plate, specifically its group index difference Δn_g for ordinary and extraordinary polarization light, can be tuned for achieving single-aperture, alignment-tolerant stimulated emission depletion (STED) nanoscopy with versatile control over the color combinations as well as laser bandwidths. Point spread function measurements reveal the ability to achieve single-aperture STED illumination systems with high throughput (transmission >89%) and purity (donut beam extinction ratios as high as $|-18.75|$ dB, i.e., ~1% residual light in the dark center of the donut beam) for a variety of color combinations covering the entire visible spectrum, hence addressing several of the fluorescent dyes of interest in STED microscopy. In addition, we demonstrate dual-color STED illumination that would enable multiplexed imaging modalities as well as schemes that could use wide bandwidths up to 19 nm (and hence ultrashort pulses down to ~50 fs). Switching between any of these color settings only involves changing the bias of the q-plate that does not alter the alignment of the system, hence potentially facilitating alignment-free, spectrally diverse multiplexed nanoscale imaging.

OCIS codes: (140.3300) Laser beam shaping; (060.2350) Fiber optics imaging; (180.2520) Fluorescence microscopy.

http://dx.doi.org/10.1364/OPTICA.2.000900

Stimulated emission depletion (STED) microscopy is one of the most successful far-field imaging techniques to date, allowing access to resolution beyond the diffraction limit [1,2]. It uses a Gaussian-like beam to excite the fluorophore and a red-shifted, spatially overlapped donut-shaped beam to deplete the fluorescence everywhere except at the dark center of the depletion beam. The resolution is critically influenced by the quality of the intensity null at the center of the donut beam, often called the STED beam, at focus, since any residual light or misalignment of the dark central region directly mitigates the depletion effect that yields nanoscale resolution. To achieve a high-quality donut beam, it is well known that vortex modes with orbital angular momentum (OAM) or, equivalently, helical phase are required, and it is critical that the handedness for both the helical phase and circular polarization be the same [3]. Such beams are also called spin-orbit aligned OAM beams [4].

STED microscopy, while a very attractive technique for realizing super-resolution, suffers from practical drawbacks: the STED beam needs to be a pure spin-orbit aligned OAM beam and the Gaussian excitation and STED beam need to be spatially coaligned with very high precision. Hence, the performance of STED systems is susceptible to thermal variations and vibrations, currently limiting their deployment in clinical environments. Solutions for addressing these alignment concerns include: (a) vortex fibers whose eigenmodes stably deliver STED as well as Gaussian beams of different colors from a single fiber aperture [5,6] and (b) dual-wedge spiral phase plates [7] or segmented waveplates [8] with engineered dispersion to enable specific color combinations. However, the free-space solutions, while addressing the alignment problem, come with inherent bandwidth limitations [9]. The excitation beam becomes highly non-Gaussian barely 50 nm away from the design wavelength, and STED beam bandwidths greater than a few nm remain infeasible.

In this Letter, we show that the q-plate, in contrast, is a free-space device that can address the alignment tolerances of STED while also enabling broadband or multicolor operation. Q-plates [10,11] are liquid crystal (LC)-based devices that have uniform birefringence-induced phase retardation $\Delta\delta$ but an inhomogeneous orientation of the fast axis of LC cells such that control of the input polarization of a conventional Gaussian beam can yield a variety of OAM eigenmodes of free-space or a fiber [12]. The conversion efficiency is determined by $\Delta\delta$, which is determined by the dispersive properties of the LCs. Typically, $\Delta\delta$ can be tuned by temperature, electric field [13], or pressure, and is wavelength dependent; this large dispersion space may be beneficially exploited for building

2334-2536/15/100900-04$15/0$15.00

Corrected 12 November 2015

STED microscopes whose illumination characteristics are simply controlled by a bias voltage and input polarization.

The measured point spread function (PSF) results of the single-aperture STED system we built using a $q = 1/2$ plate reveal that STED beam bandwidths as high as 19 nm, corresponding to ultrashort pulses as short as 50 fs, are achievable. Moreover, the AC bias voltage-based control of $\Delta\delta$ as well as its chromatic dispersion (specifically the group refractive index difference, Δn_g, between ordinary and extraordinary light passing through the LC waveplate) enables realization of STED-Gaussian beam pairs (and even multicolor combinations) ranging from 480 to 775 nm without having to physically realign the system.

The Jones matrix describing the local behavior of a q-plate with a general phase retardation $\Delta\delta$ for a rotation matrix $R(\alpha)$, where $\alpha = \alpha(r,\varphi) = q\varphi + \alpha_0$, and q and α_0 are constants that describe the distribution of the LC cells' fast axes, is given by [10]

$$\boldsymbol{M}(\varphi) = \boldsymbol{R}(\alpha)\begin{pmatrix} 1 & 0 \\ 0 & e^{i\Delta\delta} \end{pmatrix}\boldsymbol{R}(-\alpha), \tag{1}$$

where φ is the azimuthal polar coordinate in the q-plate plane. For a circularly polarized input $\hat{\sigma}^{\pm}$ (+ and – representing left- and right-handed circular polarization, respectively) the normalized output field can be derived as

$$\boldsymbol{E}_{out} = \boldsymbol{M}\bullet\hat{\sigma}^{\pm} = \frac{1}{2}[(1+e^{i\Delta\delta})\hat{\sigma}^{\pm} + (1-e^{i\Delta\delta})\hat{\sigma}^{\mp}e^{\pm i(2q\varphi+2\alpha_0)}] \tag{2}$$

(see Fig. S1, Supplement 1, Section 1 for output fields for all input polarizations).

Thus, the output field is a superposition of a Gaussian beam (first term in square brackets) of the same polarization as the input and an OAM beam of the opposite polarization, with topological charge $2q$ of the OAM beam determined by input polarization. The weight of the Gaussian beam is then given by

$$I_{Gau} \propto \frac{1}{2}|1+e^{i\Delta\delta}|^2 = \cos^2\frac{\Delta\delta}{2}. \tag{3}$$

Similarly, the weight of the OAM beam (that after being converted into a spin-orbit aligned state can be used as STED beam) produced at the output also oscillates with $\Delta\delta$, in a manner complementary to the weight of the Gaussian. Note that $\Delta\delta$ is a function of the difference in the extraordinary and ordinary refractive indices n_e and n_o, corresponding to linear polarization states $\hat{x}$ and $\hat{y}$, respectively. Thus, it is a function of both bias applied on the LC and wavelength. Specifically, we could write the wavelength dependence of $\Delta\delta$ as a Taylor series about some central frequency ω_0 [14] (see also Supplement 1, Section 2):

$$\Delta\delta(V,\omega) = \Delta\boldsymbol{k}\bullet\boldsymbol{d} = \boldsymbol{d}\bullet\left[\frac{1}{c}\Delta\boldsymbol{n_g}(V,\omega_0)\bullet\Delta\boldsymbol{\omega} + \frac{1}{2!}\Delta\boldsymbol{k''}\bullet\Delta\boldsymbol{\omega}^2\ldots\boldsymbol{O}(\Delta\boldsymbol{\omega}^n)\right], \tag{4}$$

where c is the speed of light in free space, $\Delta k = (n_e - n_o)\bullet\omega/c$, d is the thickness of the q-plate, $\Delta\omega = \omega - \omega_0$, Δn_g is the group index difference between $\hat{x}$ and $\hat{y}$ (the first Taylor order, since $\Delta k' = \Delta n_g/c$), $\Delta k''$ is the difference of the second-order derivative of the wavenumbers (i.e., difference in group-velocity dispersion between the two polarization axes; see [14] for more details), and $O(\Delta\omega^n)$ represents higher-order corrections.

Figure 1 shows camera images of collimated Gaussian beams of two different colors passing through a $q = 1/2$ plate at multiple bias settings. Clearly, the appearance of a Gaussian or OAM beam appears to have an oscillatory dependence on bias

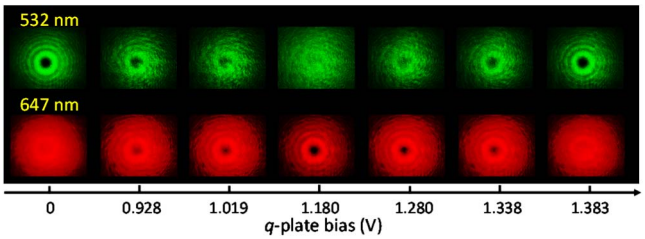

Fig. 1. Free-space images of two beams of different wavelengths passing through a $q = 1/2$ plate at different voltage biases.

or wavelength, as suggested by Eqs. (2)–(4). To quantify the extent to which the beam is Gaussian-like or carries OAM we start by noting that, at the beam center, only a Gaussian beam can contribute to a nonzero intensity value. Hence, we define an extinction ratio (ER; zero for an OAM and unity for a Gaussian mode) by measuring the ratio of the intensity at the beam center (see Supplement 1, Section 3, Fig. S2) with and without the q-plate in the beam path. This extinction ratio is recorded as we change the wavelength of the input beam from a laser with full-width half-maximum bandwidth of 3 nm (Solea, PicoQuant); Fig. 2 shows one such curve for 1.18 V bias.

We see that (1) for a certain bias, the output is Gaussian at one wavelength (e.g., 532 nm, see the green mode image) and OAM at another (e.g., 647 nm, see the red mode image); (2) the oscillation frequency ($\Delta\omega_p$, where $2\pi * \Delta\omega_p/2$ is depicted in Fig. 2; see Supplement 1, Section 2 for more information) appears unchanged over this wavelength range (480–700 nm). This implies that the difference between the two orthogonal polarization axes in group velocity dispersion and any other higher-order dispersive terms $d\bullet\Delta k''$, $d\bullet O(\Delta\omega^n)$ is negligible, consistent with the expectation that group-velocity dispersion differences between two polarization axes would be small in a thin birefringent waveplate.

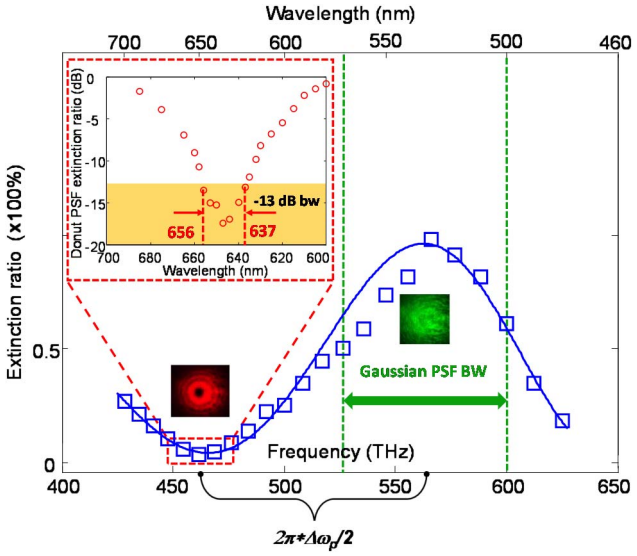

Fig. 2. Extinction ratio as a function of wavelength, with bias of 1.180 V. OAM (red) and Gaussian (green) mode images are also shown. The green dashed vertical lines mark out the wavelength range over which a Gaussian beam PSF can be obtained. Inset: extinction ratio of the donut PSF as a function of wavelength. Red arrows indicate the –13 dB bandwidth (BW).

Therefore, it is safe to rewrite Eq. (4) as $\Delta\delta \cong d/c \bullet \Delta n_g(V,\omega_0) \bullet \Delta\omega$, and hence the extinction ratio is oscillatory with frequency, with period $\Delta\omega_p$ such that $\Delta\delta(V, \Delta\omega_p) = \pi$.

Combining the just-discussed equation and Eq. (3), and by fitting the data (measured at several biases) to $\cos^2(a\omega)$ (solid line in Fig. 2), where $\omega/2\pi$ is the optical frequency and a is a fitting parameter, we can calculate Δn_g for the LC waveplate. For different biases, OAM beams with 98.4% purity (−18 dB extinction ratio) may be obtained across the visible spectral range (the mode purity, and hence absolute value of the extinction ratio, may well be higher; the dynamic range of our camera limits measurements to ∼18 dB). Figure 3(a) plots the wavelengths at which full OAM mode conversion (extinction ratio → 0 in linear units, −∞ in dB) occurs versus q-plate bias voltage. Note that for certain wavelengths, "pure" OAM modes may be created at multiple bias voltages, reinforcing the oscillatory behavior predicted by Eq. (3). The spectral period at which OAM modes are created, as a function of bias voltage, is shown in Fig. 3(b) and reveal the dependence of the group-index birefringence on applied bias voltage.

Figures 3(a) and 3(b) suggest the methodology by which one may find the pairs of wavelength at which, for a given input beam and q-plate bias, one could obtain a STED (OAM) and Gaussian beam simultaneously. The bias is tuned to the wavelength at which a "pure" STED beam results, as deduced from Fig. 3(a), and it is expected that at a spectral position that is half the oscillation period for this bias [as determined from Fig. 3(b)], one would obtain a Gaussian beam. This yields a single-aperture STED illumination setup that is tunable across the visible spectral range, though with restrictions on the wavelength separation between the STED and Gaussian beams. As we will show later, the system is, in fact, significantly more adjustable/tunable because while Fig. 3 traces the spectral positions at which highly pure STED or Gaussian beams are obtained, there is a finite bandwidth over which the beams remain useful for STED.

To obtain a realistic measure of this performance, we use a home-built confocal laser scanning microscopy setup to characterize the PSF of the beams created by these devices (Fig. 4 shows setup schematic; see Supplement 1, Section 3 for details).

Figure 5(a) shows the results from the implementation of single-aperture STED illumination with a Gaussian excitation at $\lambda = 532$ nm and STED at $\lambda = 647$ nm. Two-dimensional PSFs in the lateral and axial directions are shown in Fig. 5(a), and free-space mode images obtained from the q-plate are shown in Fig. 5(b) (all with false colors corresponding to the respective wavelengths of illumination). We obtained a donut PSF extinction ratio of −18.75 dB [Fig. 5(c), plotted in linear scale for visual clarity; corresponding log scale plot shown in Fig. S4]. This

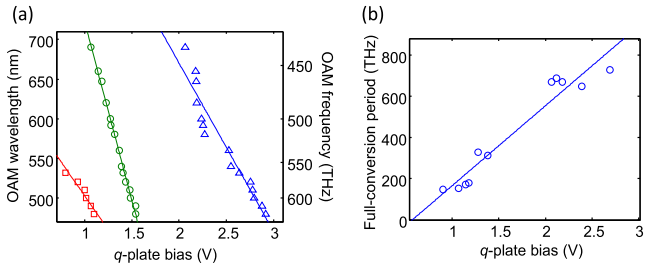

Fig. 3. (a) OAM full-conversion wavelength (and frequency) as a function of the q-plate bias; (b) full-conversion period in frequency as a function of the q-plate bias.

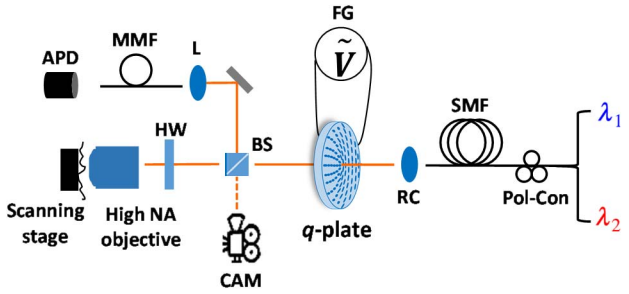

Fig. 4. Experimental setup. Pol-Con: fiber polarization controller; RC: reflective collimator; FG: function generator; CAM: CMOS camera; BS: beam splitter; L: lens; MMF: multimode fiber; APD: avalanche photodiode; HW: $\lambda/2$ plate. See Supplement 1, Section 3 for additional experimental details.

significantly exceeds the −13 dB requirement (5% of intensity in the dark center compared to the peak of the STED beam) often quoted as desirable for STED microscopy [15].

Next, we study the bandwidth of our single-aperture system. We fix the q-plate bias to have the largest vortex extinction ratio at 647 nm and record PSFs while sweeping the central wavelength from 600 to 690 nm. The extinction ratio for the STED beam as a function of center wavelength, shown in the inset of Fig. 2, remains below the −13 dB metric across 19 nm (637–656 nm). This is consistent with our observation, in parallel, that at the center wavelength of 647 nm, the extinction ratio remains smaller than −13 dB for all bandwidth settings (3–15 nm) available from the laser (Solea, PicoQuant) we tested.

Intuitively, from Fig. 2, we expect that the bandwidth where we could obtain a Gaussian PSF (at the complementary wavelengths around 532 nm) would be similar. However, measurements of the PSF at around 532 nm reveal that the overlap integral of the line-cut profile of the PSF with that of a pure Gaussian beam PSF (i.e., a *Jinc* function), degrades by less than 1% as long as the free-space extinction ratio remains larger than −3 dB (see Supplement 1, Section 3, Fig. S3 for details of this calculation). Thus, our experiments reveal a Gaussian PSF bandwidth of ∼60 nm, considerably larger than that for the STED beam. This points to the feasibility of dual or multicolor STED (where a variety of Gaussian excitation beams may be deployed for multiplexed imaging).

Figures 5(d)–5(g) show corresponding PSFs, free-space images, and PSF extinction plots for an exemplary demonstration of dual-color STED. The q-plate bias is set at 1.28 V, STED $\lambda = 592$ nm, but two Gaussian excitation beams at $\lambda = 488$ and 514 nm are simultaneously deployed. The measured donut PSF vortex extinction ratio was −14.11 dB which, though better than that required for STED microscopy [15], is nevertheless degraded compared to the single-color experiment of Figs. 5(a)–5(c). However, we believe this is due not to the dual-color aspect of the experiment but rather to our measurement limitations. The 150 nm gold beads used for our PSF measurements are similar in size to that of the dark center (theoretically calculated to be 119 nm) for the STED beam at $\lambda = 592$ nm; hence, using smaller gold beads would have yielded deeper PSF extinction ratios, especially since we did not see any apparent degradation in the mode purity of the free-space STED beams obtained from the q-plate across the entire wavelength range we tested.

All colors came out of a single-aperture (fiber and q-plate), as shown in Fig. 4, reinforcing the alignment simplicity of this setup.

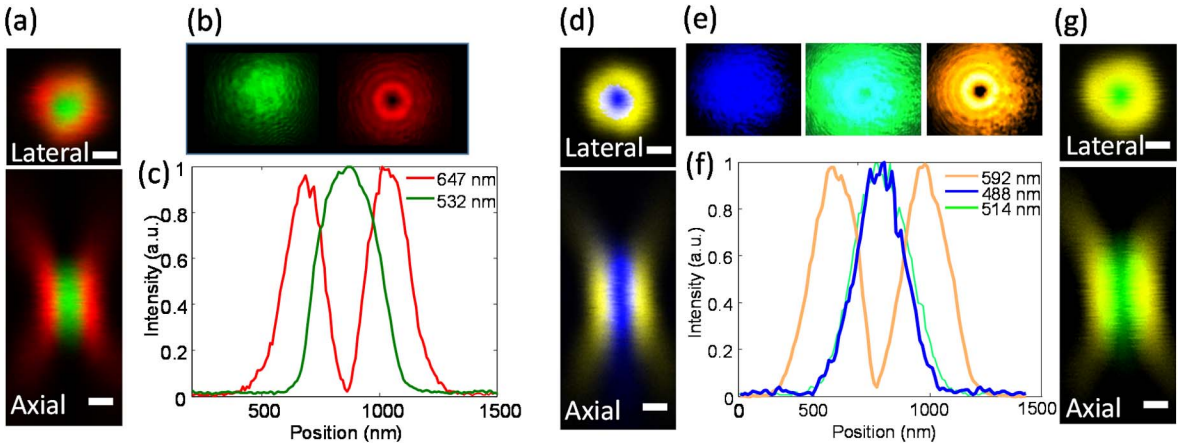

Fig. 5. PSFs for (a) 532 nm Gaussian and 647 nm STED beams with bias = 1.180 V; (d) and (g) 488 nm and 514 nm Gaussian and 592 nm STED beams with bias = 1.280 V, in lateral and axial planes. The corresponding free-space mode images are shown in (b) and (e), and the central line cut profiles of lateral PSFs are shown in (c) and (f), respectively. Scale bar: 200 nm.

Moreover, no physical realignment was needed when switching across all these wavelength combinations, spanning RGB of the visible spectrum. We repeated these PSF measurements for a range of color combinations that address commonly used fluorescent dyes and the results (see Supplement 1, Fig. S4), along with the dye for which each experiment may be suitable, are illustrated in Table 1 ("n/a" signifies laser wavelengths not available for testing). Finally, the measured loss of the q-plate was less than 0.5 dB (transmission >89%; see Supplement 1, Fig. S5) across the entire wavelength range, underscoring the utility of these devices for applications with powerful STED beams.

In summary, a single-aperture STED illumination system using a high-throughput (transmission >89%) q-plate and a single-mode fiber is demonstrated. The q-plate acts as an OAM mode converter, spatially modifying the laser beams of different colors in a wavelength-dependent fashion. This arises from the dependence of the group index difference of the q-plate on the bias voltage and wavelength, and thus allows easy tuning of the depletion wavelength without changing the optical alignment of the system. The operation bandwidth for practical STED implementation is measured to be 19 nm, considerably larger than that of other single-aperture techniques. The even larger bandwidth for Gaussian PSFs enables dual-color or even multicolor implementation over a variety of wavelength ranges. Even more dramatic improvements in Gaussian PSF bandwidth may be obtained by including polarization optics after the q-plate, because the fundamental action of the device yields Gaussian and OAM (STED) beams of orthogonal polarizations. Based on our single-aperture results, we believe that q-plates will find important applications in CW, pulsed, or time-gated STED nanoscopy since they address the alignment-intensive nature of these systems while also providing for an alignment-free, color-tunable system enabling multicolor STED microscopy.

Table 1. STED Wavelength Combinations and Dyes [16]

Bias (V)	$\lambda_{STED}/\lambda_{exc}$ (nm)	Donut |ER| (dB)	Donut Size (nm)	Corresponding Dyes
0	532/440 458	n/a	n/a	ATTO 425 Abberior 440SX
1.289	592/488 514	14.11	119	Alexa Fluor 488 Oregon Green 488
1.180	647/532	18.75	166	ATTO 565
1.085	690/570	17.17	171	ATTO 590
1.986	750/532	16.69	175	Abberior 470SXP
0	775/594	17.18	180	ATTO 594

Funding. Defense Advanced Research Projects Agency (DARPA) (InPho); National Science Foundation (NSF) (ECCS-1310493); Canada Excellence Research Chairs Program (CERC); European Union (FP7-PEOPLE-2012-CIG, PCIG12-GA-2012-326499-FOXIDUET); National Science Foundation Graduate Research Fellowship Program (NSF-GRP) (DGE-1247312).

Acknowledgment. We thank P. Kristensen for fiber fabrication.

See Supplement 1 for supporting content.

REFERENCES

1. S. W. Hell and J. Wichmann, Opt. Lett. **19**, 780 (1994).
2. J. R. Moffitt, C. Osseforth, and J. Michaelis, Opt. Express **19**, 4242 (2011).
3. X. Hao, C. Kuang, T. Wang, and X. Liu, J. Opt. **12**, 115707 (2010).
4. S. Ramachandran, P. Gregg, P. Kristensen, and S. E. Golowich, Opt. Express **23**, 3721 (2015).
5. L. Yan, E. Auksorius, N. Bozinovic, G. J. Tearney, and S. Ramachandran, *CLEO*, OSA Technical Digest (online) (Optical Society of America, 2013), paper CTu3N.2.
6. S. Ramachandran, P. Kristensen, and M. F. Yan, Opt. Lett. **34**, 2525 (2009).
7. D. Wildanger, J. Bückers, V. Westphal, S. W. Hell, and L. Kastrup, Opt. Express **17**, 16100 (2009).
8. M. Reuss, J. Engelhardt, and S. W. Hell, Opt. Express **18**, 1049 (2010).
9. F. Gorlitz, P. Hoyer, H. Falk, L. Kastrup, J. Engelhardt, and S. W. Hell, Prog. Electromagn. Res. **147**, 57 (2014).
10. L. Marrucci, C. Manzo, and D. Paparo, Phys. Rev. Lett. **96**, 163905 (2006).
11. E. Karimi, B. Piccirillo, E. Nagali, L. Marrucci, and E. Santamato, Appl. Phys. Lett. **94**, 231124 (2009).
12. P. Gregg, M. Mirhosseini, A. Rubano, L. Marrucci, E. Karimi, R. W. Boyd, and S. Ramachandran, Opt. Lett. **40**, 1729 (2015).
13. S. Slussarenko, A. Murauski, T. Du, V. Chigrinov, L. Marrucci, and E. Santamato, Opt. Express **19**, 4085 (2011).
14. S. Ramachandran, J. Lightwave Technol. **23**, 3426 (2005).
15. K. I. Willig, R. R. Kellner, R. Medda, B. Hein, S. Jakobs, and S. W. Hell, Nat. Methods **3**, 721 (2006).
16. http://nanobiophotonics.mpibpc.mpg.de/old/dyes/.